Check for updates

Advanced Materials Interfaces

ADVANCED MATERIALS INTERFACES Open Access

www.advmatinterfaces.de

RESEARCH ARTICLE OPEN ACCESS

Cellulose Surface Modification Effects on Equilibrium and Non-Equilibrium Wetting by Water

Jakob Wohlert | Lars Berglund

Department of Fiber and Polymer Technology, KTH Royal Institute of Technology, Stockholm, Sweden

Correspondence: Jakob Wohlert (jacke@kth.se)

Received: 29 May 2026 | **Revised:** 15 September 2026 | **Accepted:** 26 September 2026

Keywords: acetylated cellulose | contact line friction | molecular dynamics simulations | TEMPO oxidized cellulose | water contact angle

ABSTRACT

Chemical modification is an important route to tuning interactions between nanocellulose and its surrounding media. Specifically, it affects the wetting characteristics, which in turn affect water transport, moisture sensitivity, and liquid processability. Wetting at the nanoscale is difficult to characterize experimentally, which is why molecular simulation is an attractive method for investigating these phenomena. However, simulations are sensitive to choice of interaction parameters and methodology. Here, we investigate wetting of both native and surface modified (acetylated and TEMPO oxidized) cellulose substrates by water in molecular dynamics simulations. Two complementary methods are compared: simulation of explicit droplet spreading, and an indirect method where the equilibrium wetting angle is given by the solid-liquid work of adhesion computed from the potential of mean force. In addition, the dynamics of wetting is analyzed within the framework of molecular kinetic theory. Our results clearly show the effects of surface modification on both the equilibrium contact angle and the wetting dynamics where hydrophobization decreases, and oxidation increases, the wetting efficiency. In addition, it is shown that contact line friction is the dominating energy dissipation mechanism for cellulose wetting at the nanometer scale.

1 | Introduction

Native cellulose molecules are organized in the form of nanofibrils. The polymer itself is a linear extended chain polysaccharide composed of β(1,4) linked β-D-glucopyranose units. The structural load-bearing fibrils (3–10 nm in diameter) are present in plant cell walls but is also produced by certain bacteria and algae, and even in rare cases by fungi and animals (tunicates). Cellulose has a long history of being used by humans and is an important material for the establishment of civilizations [1]. It has been used in the form of wood for construction, tools and weapons, fibers for structural joints, water transportation, textiles and paper. Recently structures at the nanoscale have been used to make biocomposites based on isolated cellulose nanofibrils, or exploited in the emerging field of wood nanotechnology [2].

The interaction between cellulose and water is important from a fundamental point of view, for instance to understand the properties of the hydrated plant cell wall, as well as in most practical applications involving cellulose-based materials [3–5]. The chemical structure of cellulose molecules results in fibril surfaces with a high density of available hydroxyl groups, ideal for favorable interaction with water molecules. In addition, due to its fibrillar building blocks, cellulose materials have porous structures with cavities that range from microscopic, such as the lumen in wood cells, all the way down to nanometers and below in networks created by isolated cellulose nanofibrils in, for instance, cellulose nanopaper [6]. Even these nanometer-sized voids are sufficiently large to accommodate water molecules [7]. As a consequence, cellulose materials swell in contact with liquid water or air with high relative humidity, which from a materials perspective leads to poor dimensional stability and

This is an open access article under the terms of the Creative Commons Attribution License, which permits use, distribution and reproduction in any medium, provided the original work is properly cited.

© 2026 The Author(s). *Advanced Materials Interfaces* published by Wiley-VCH GmbH

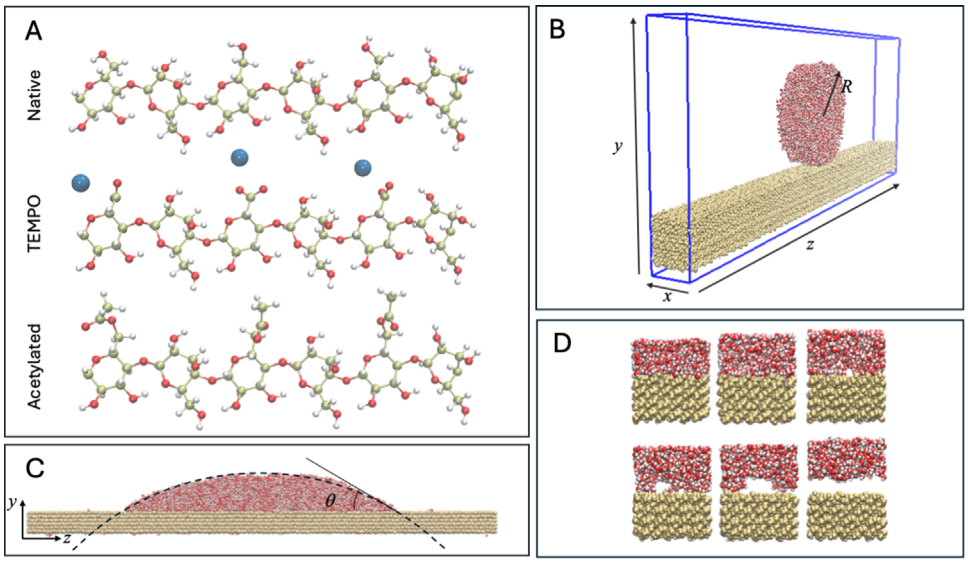

FIGURE 1 | Description of system setups. (A) The chemical structure of Native, TEMPO oxidized (with Na^+ counter ions), and Acetylated cellulose, (B) quasi-2D system for simulations of droplet spreading, (C) Definition of the contact angle, and (D) slab geometry used for PMF calculations shown at increasing liquid-solid separation.

varying mechanical properties. In addition, cellulose materials are difficult to dry, and even the most careful drying protocol will leave detectable amounts of water [8]. As a consequence, even oven-dried cellulose materials will have water present at internal cellulosic surfaces under ambient conditions, which, for the case of polymer matrix composites, will influence the interaction of cellulose fibers with monomers and oligomers during processing.

Cellulose can be chemically modified by replacing chemically accessible hydroxyl groups on its free surfaces with other functionalities [9, 10]. Materials from chemically modified nanocellulose are used industrially, and the purpose of the modification is to enhance its properties, such as optical transparency or mechanical properties [11], to increase dispersibility of cellulose nanofibrils [12], to increase the compatibility of cellulose nanoparticles with a polymer matrix for composite processing [13], or to reduce moisture sensitivity [14]. However, the molecular scale interactions behind these phenomena are still not well understood.

Studies of cellulose and water at the nanoscale require extreme spatial and temporal resolution, which makes computer simulation, specifically molecular dynamics (MD), an attractive option. In fact, computer simulations have shown that the presence of water in nanosized pores decreases the total free energy in equilibrium [15, 16], explaining why trace amounts of water are always present in cellulose under normal temperature and relative humidity. MD also provides a means to understand cellulose-water interactions in the framework of thermodynamics. An important way to characterize solid-liquid interactions is through the concept of contact angles. A liquid drop spreading on a solid substrate will eventually (if evaporation is neglected) either wet the surface completely or stop spreading with the droplet forming a finite contact angle, θ, with the solid (Figure 1C). The contact angle is a consequence of a balancing the thermodynamic surface forces given by Young's equation,

$$\gamma \cos\theta = \gamma_S - \gamma_{SL} \quad (1)$$

where γ is the liquid surface tension, γ_S is the solid surface energy and γ_{SL} is the surface energy of the solid-liquid interface. Wetting is thus promoted by a large (positive) difference $\gamma_S - \gamma_{SL} \equiv \Delta\gamma$ and a small surface tension. This can be expressed via the spreading coefficient, $S = \Delta\gamma - \gamma$, where complete wetting is achieved for $S \geq 0$ [17]. Contact angle measurements have been used extensively to characterize different cellulose surfaces, and the literature gives values of $\theta = 15°–47°$ for untreated nanocellulose films [18–23]. However, the macroscopic contact angle determined experimentally is influenced by effects such as surface roughness, impurities, and other types of chemical and structural heterogeneity. Together with a strong tendency of cellulose substrates to absorb water, this makes it difficult to extrapolate to predict nanoscale wettability. MD simulations, on the other hand can model the spreading of nanosized droplets over ideal, smooth model substrates and has been used to predict cellulose wettability in several studies [24–29]. In addition, surface energies and contact angles from MD simulations are useful as input to simulations on larger scales, such as computational fluid dynamics. MD results, however, depend heavily on the empirical potential energy function used for cellulose and even more on the choice of water model. They are also complicated by finite size effects and slow convergence, which means that simulations risk being both too small and too short. The finite size of the droplet can affect the observed contact angle in at least two ways. First, at the nanoscale, the curvature of the contact line for a 3D droplet on a solid surface is high, leading to a significant contribution from line tension to the mechanical equilibrium. This effect can be removed by employing a 2D geometry (cylindrical droplets) where the curvature of the contact line is zero. However, even in this geometry, there is a contribution from the curvature of the liquid-vapor interface to γ [30], which can affect the contact

21967350, 0, Downloaded from https://advanced.onlinelibrary.wiley.com/doi/10.1002/admi.70698 by CochraneItalia, Wiley Online Library on [07/10/2026]. See the Terms and Conditions (https://onlinelibrary.wiley.com/terms-and-conditions) on Wiley Online Library for rules of use; OA articles are governed by the applicable Creative Commons License

angle in MD simulations for droplets up to several nm in size [31]. Second, since the spatial resolution is limited by the size of the water molecules and thermal fluctuations of the liquid-air interface increase at the nanoscale, large droplets are needed to get an accurate reading of the contact angle when θ is small. There are many potential sources of error and consequently reported simulated values range from 0° to 70° for hydrophilic faces of cellulose. For this reason, there is no consensus around the simple question of whether water, at the nanoscale, wets cellulose completely or not.

A straightforward way to address the finite size effects is naturally to increase the system size. For example, a droplet radius of 5 nm and a slab thickness of 4 nm amounts to 10 000 water molecules, and doubling the size to 10 nm thus gives 40 000 molecules, which is still perfectly within range for atomistic simulation. Indeed, water droplets as large as one million water molecules have been simulated in atomistic detail [32]. However, this is not an effective approach for systematic studies. There exist several methods that can be used with MD to compute surface energies [33], for example Kirkwood–Buff theory [34] for liquid-liquid interfaces, or the capillary fluctuations method [35] for solid-liquid coexistence. One alternative method, which is explored here, is to use steered MD to compute the work of adhesion, W_A, between the solid and the liquid from the potential of mean force when separating the two phases [25]. The adhesion is a measure of interaction and can be connected to the contact angle through the Young–Dupré equation,

$$W_A = \gamma\,(1 + \cos\theta) \tag{2}$$

The main advantage of this approach is that it removes the possible dependence of the measured contact angle on finite droplet size.

In this study, we investigate how cellulose wettability depends on the chemical nature of the cellulose substrate. We compare acetylation, which lowers moisture sorption and provides hydrophobicity [14], TEMPO-oxidation, which introduces surface charge through electronegative carboxylates [36], and two different native crystal planes (often termed "hydrophobic" and "hydrophilic"). We use MD simulations of larger water droplets and longer simulation times than in previous cellulose-water studies. In addition, we compare results from the large-scale droplet simulations with the adhesion calculated from the potential of mean force (PMF), which we hypothesize could be used to decrease the computational effort. Finally, we investigate the dynamics of wetting and how it is affected by surface chemistry, and the timescales needed to achieve converged contact angle measurements from the simulations.

2 | Methods

2.1 | Simulation Setup

The simulations used fully atomistic models based on the GLYCAM06 force field [37] for carbohydrates and the SPC/E model [38] for water. The cellulose substrates were constructed from the native cellulose Iβ crystal structure, facing either the hydrophilic (110) or the hydrophobic (100) face towards the liquid. These surfaces are denoted Native hydrophilic and Native hydrophobic, respectively. In addition to native cellulose, two models of chemically modified cellulose were used (Figure 1A), where the surface residues were either fully acetylated in the C6 position, or fully carboxylated, mimicking the effect of TEMPO oxidation [39]. Note that fully substituted here means that every second glucose residue on the surface was modified, since every other C6 hydroxyl points into the crystal due to the twofold helical screw of the glucan chain, making them inaccessible for chemical reactions. In addition, only the (110) surface was modified. The carboxylates were modeled in their negatively charged deprotonated form, and to neutralize the system a number of Na^+ ions [40] were added, initially placed close to the carboxylates.

All simulations were performed using GROMACS [41] with a Verlet integrator and a basic time step of 2 fs. All bonds were kept at their equilibrium lengths using P-LINCS [42]. Non-bonded interactions used a cut off of 1.2 nm and long-range electrostatics were included using particle mesh Ewald summation (PME) [43, 44]. Simulations were performed in the NVT ensemble where the water and the cellulose were separately coupled to a thermal reservoir of temperature 300 K using stochastic velocity-rescaling [45] with a time constant of 2 ps.

2.2 | Contact Angle Determination

The most straightforward approach to compute contact angles from atomistic simulations is to simply put a droplet of liquid on a substrate and let it spread until the contact line has stopped advancing. To decrease the computational effort, a quasi 2D representation was used, where the droplet initially was represented by a thin slice of a cylinder put on top of a substrate that is extended in one dimension only and kept relatively small in the other two (Figure 1B). The cellulose substrate was composed by glucan chains aligned with the z axis, 96 residues (49.82 nm) long in a six by six ($y \times x$) arrangement, having either the hydrophilic (110) or the hydrophobic (100) plane facing the y direction. The initial radius of the droplets used here was $R = 5$ nm, and the thickness (x) was 3.58 nm for the hydrophilic (110) surfaces and 2.28 nm for the hydrophobic (100) surface, respectively. The contact angle was measured in the post-processing of the simulation trajectories by tracing the density contour of the liquid and fitting it by an arc (Figure 1C and Supporting Information).

In addition to the droplet simulations, a set of simulations were performed where a slab of water was placed on top of a slab of cellulose (Figure 1D), native or chemically modified. The substrate consisted of four layers of six chains each, and each chain was composed of six monomers. The water layer was approx. 1.8 nm thick and consisted of 653 molecules. The two phases were subsequently separated along the y axis using umbrella sampling on distance between their respective centers of mass. To keep the water phase intact a flat bottom position restraint was employed, in the y direction only. The width of the potential well used for the restraints was 2.2 nm, i.e., larger than the thickness of the water slab to minimize the interference at the two end points. The umbrella sampling was performed using 25 umbrella windows where the reference position was increased in steps of 0.05 nm. The force constant for the umbrella potential was 50 000 kJ

21967350, 0, Downloaded from https://advanced.onlinelibrary.wiley.com/doi/10.1002/admi.70698 by CochraneItalia, Wiley Online Library on [07/10/2026]. See the Terms and Conditions (https://onlinelibrary.wiley.com/terms-and-conditions) on Wiley Online Library for rules of use; OA articles are governed by the applicable Creative Commons License

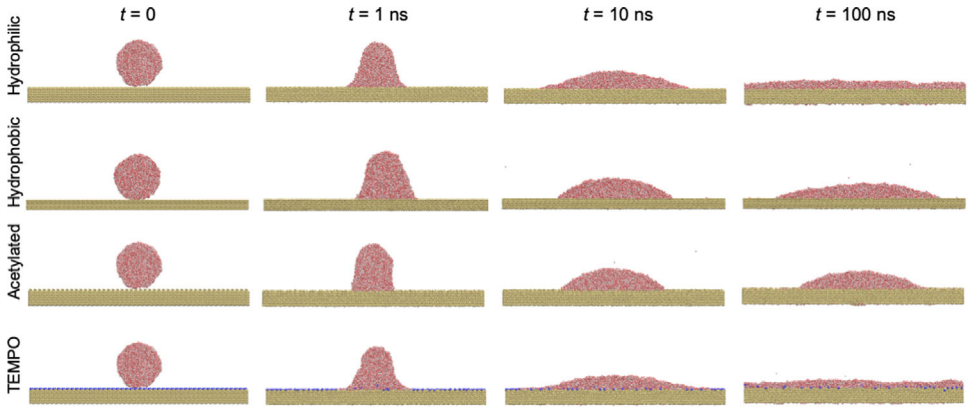

FIGURE 2 | Snapshots of a water droplet (initial radius 5 nm) spreading on cellulose surfaces of different chemistries. "TEMPO" and "Acetylated" are chemically modified whereas "Hydrophobic" (100) and "Hydrophilic" (110) correspond to different surfaces in native cellulose I.

mol^{-1} nm^{-2}. For each reference position a 20 ns (hydrophobic surfaces) or 40 ns (hydrophilic surfaces) long simulation was performed. The umbrella simulations were connected using the weighted histogram analysis method (WHAM), which gives the equilibrium free energy as a function of the separation. The free energy difference between the end points (normalized by the area) is the work of adhesion, W_A.

The instantaneous liquid surface tension of water was calculated as usual from the diagonal components of the pressure tensor from a single water slab simulated at constant volume [34],

$$\gamma(t) = \frac{L_z}{2}\left(P_{zz}(t) - \frac{1}{2}\left(P_{xx}(t) + P_{yy}(t)\right)\right) \quad (3)$$

The slab consisted of 2200 water molecules and were simulated for 10 ns.

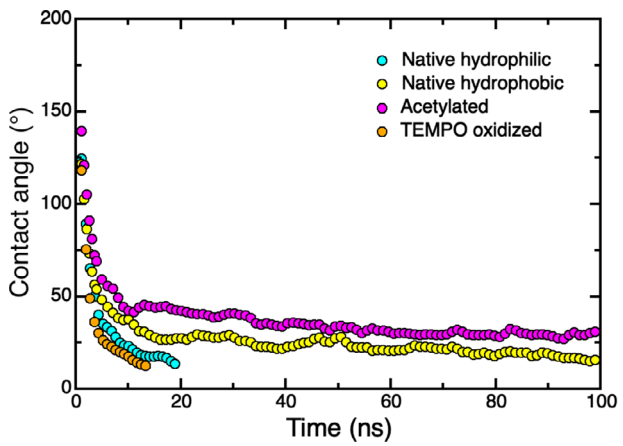

FIGURE 3 | Contact angles as a function of simulation time for water droplets on native and chemically modified cellulose surfaces. Data points represent averages over 1 ns.

3 | Results and Discussion

3.1 | Equilibrium Wetting of Cellulose Surfaces From Droplet Simulations – The Explicit Method

The static contact angle depends on liquid/solid interactions and is highly relevant for understanding moisture sorption in nanocellulose materials, where also nanoscale porosity and specific surface area influence results. It is important to simulate static wetting under conditions of equilibrium, meaning that simulations need to be sufficiently long for the contact angle to develop. Some previous studies may suffer from short simulation times so that equilibrium has not been reached. Figure 2 shows the time evolution of a water droplet of initial radius $R = 5$ nm spreading on cellulose substrates. All four droplets exhibit similar features during the first few nanoseconds, although the exact shape varies due to large fluctuations, and after about 10 ns the familiar shape of a sessile liquid drop on a solid substrate has developed in all cases. However, these droplets are not yet stabilized, which is evidenced by the fact that during the following 90 ns the droplets continue to spread. After a long time (100 ns) there is a distinct difference between hydrophilic (Native hydrophilic and TEMPO-oxidized) and hydrophobic cellulose (Native hydrophobic and Acetylated). In the former case, the liquid water wets the surfaces completely, while in the latter case a finite contact angle has formed. From the simulation trajectories the contact angles were calculated as a function of time (Figure 3). The hydrophobic surfaces show much slower decrease in contact angle and maintain a finite contact angle even after long simulation time. The more hydrophilic surfaces show rapid decrease in contact angle, followed by complete wetting. The TEMPO surface shows the most rapid decrease.

The terms hydrophilic and hydrophobic need to be qualified. For the case of water, the convention is that surfaces that give $\theta > 90°$ are termed hydrophobic, whereas $\theta < 90°$ means that the surface is hydrophilic. Based on this convention, all surfaces used here are hydrophilic. Still, the (100) surface of cellulose, which differs from the (110) and the similar (1-10) surfaces in that they have restricted accessibility of the polar hydroxyl groups, is commonly denoted the "hydrophobic" face of cellulose. In addition, exchanging surface hydroxyls for acetyl groups is considered a "hydrophobization", a notion supported by the droplets shown in Figure 2. For reasons of simplicity, we will continue to refer to these surfaces as "hydrophobic" to distinguish them from the more hydrophilic (110) surface and the charged TEMPO oxidized surface.

21967350, 0, Downloaded from https://advanced.onlinelibrary.wiley.com/doi/10.1002/admi.70698 by CochraneItalia, Wiley Online Library on [07/10/2026]. See the Terms and Conditions (https://onlinelibrary.wiley.com/terms-and-conditions) on Wiley Online Library for rules of use; OA articles are governed by the applicable Creative Commons License

There are a few drawbacks of using explicit droplet simulations. The accuracy in the contact angle determination becomes limited by the liquid molecule size and thermal fluctuations of the liquid-vapor interface when θ is small. In the present case, the algorithm to determine θ becomes unreliable when the contact angle is smaller than approx. 10°. Therefore, the curves for the hydrophilic and charged surfaces are cut off close to the point where the contact line is meeting the periodic boundary. The only way to increase the accuracy is to make the droplet larger by including more liquid molecules, which also requires a larger substrate. This is a major drawback considering that even if the droplet size is "only" 5 nm, the substrate dimension is 50 nm (in its largest dimension) and the total number of atoms is more than 100 000. In addition, the slow contact line motion when the droplet is approaching equilibrium calls for long simulations to assure that the true equilibrium contact angle is obtained. The combination of large systems and long simulations is problematic. Indeed, previous MD studies of cellulose wetting were restricted in both size (droplet radii up to 2.5 nm) and time (less than 50 ns), and such restrictions may be too computationally demanding to overcome in many cases. For these reasons, a different method to investigate contact angles in the "partial to complete wetting" regime is explored in the next section.

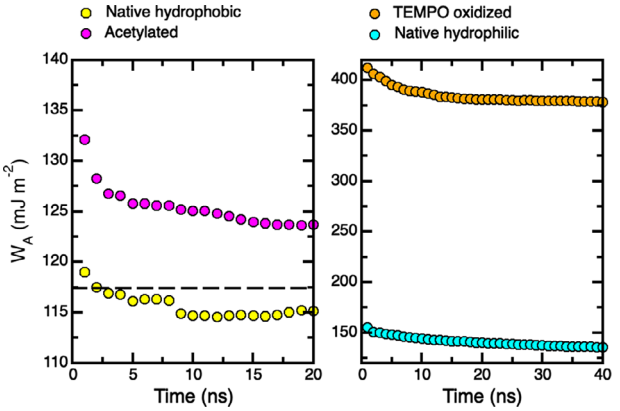

FIGURE 4 | Work of adhesion W_A from potential of mean force calculations for water on cellulose substrates as a function of the simulation time in each umbrella window, respectively. Note that the scales are different for the two diagrams since hydrophilic (TEMPO oxidized, Native hydrophilic) surfaces show much higher W_A. The dashed line marks the threshold for complete wetting, $W_A \geq 2\gamma$.

3.2 | Equilibrium Wetting From Work of Adhesion and the Potential of Mean Force – The Implicit Method

Equation 2 relates the work of adhesion (W_A) to the wetting angle θ. This work is the equilibrium (free) energy of separating the liquid from the solid and creating two new solid/vacuum and liquid/vacuum interfaces. The work of adhesion is related to the potential of mean force (PMF) along a reaction coordinate z, which should be chosen such that it reflects the separation between the liquid and the solid phase. Here, z was chosen as the center-of-mass distance between the water and the cellulose in the direction perpendicular to their original interface (Figure 1 and Methods). The PMF was calculated using umbrella sampling. An important methodological remark is that the system size compared to the droplet simulations was significantly reduced, from 100 000 atoms to around 10 000 atoms.

The objective is to investigate effects from chemically different cellulose surfaces, but the accuracy of this method needs some attention. First, it is important to investigate the simulation time for converged results. With umbrella sampling, the system is simulated at several points (umbrella windows) along the reaction coordinate. Here, a total of 48 points were used, each one simulated for the same amount of time – 20 ns for the hydrophobic surfaces and 40 ns for the hydrophilic ones (see Methods). Figure 4 displays the work of adhesion calculated from the PMF versus the portion of the trajectory (in each umbrella window) used in the analysis (with the first 25% always discarded for equilibration). These curves initially decrease with simulation time and then level off to a seemingly stable value. The time needed to reach equilibrium varies between the systems. For Native hydrophobic surface, the lower limit is ~10 ns, while at least 15–20 ns is required for Acetylated and TEMPO-oxidized surfaces. For Native hydrophilic surface, the value is still slightly decreasing after 40 ns. Thus, there is no single recommended value for the simulation time using this method, instead it should be considered from case to case, and it is expected to depend also on the choice of liquid. In addition to convergence considerations, there is a statistical error in the calculation of the PMF. Using the bootstrap analysis available in Gromacs' WHAM implementation [46] (with 50 bootstraps), this was estimated to below 1% using the full trajectories from the umbrella sampling simulations.

To calculate theta from W_A also the liquid surface tension of water, γ, is needed. Note that this refers to the surface tension of the specific water model used in the PMF simulations, at the same simulation conditions. Here, the water surface tension was calculated to 58.7 mJ m^{-2} at the present temperature, in agreement with reported literature values [28, 47]. From Equation 2 it is clear that partial wetting ($0 \leq \cos\theta \leq 1$) requires $\gamma \leq W_A \leq 2\gamma$. The lower limit for complete wetting is indicated in Figure 4 (dashed line). Only the PMF for Native hydrophobic surface falls below this value, whereas the other surfaces are all above, implying complete wetting. This agrees with the droplet simulations for the hydrophilic surfaces, but not for the acetylated surface, which in Table 1 gave a static contact angle of 30° using the previous droplet method.

All calculated contact angles from both methods, and W_A from the PMFs are summarized in Table 1. In addition, the quantities $\Delta\gamma/\gamma$ (where $\Delta\gamma \equiv \gamma_S - \gamma_{SL}$) and the spreading coefficient $S = \Delta\gamma - \gamma$ are given, which can both be viewed as measures of the thermodynamic "driving force" for wetting. Recall that Young's equation (Equation 1) is only defined for $S \leq 0$, in which case $\Delta\gamma/\gamma = \cos\theta$. While the droplet simulations cannot distinguish between the equilibrium wetting of the hydrophilic and the charged surfaces (both having $\theta = 0°$) the PMF method can since it is not restricted by $S \leq 0$ (or, equivalently, $\Delta\gamma/\gamma \leq 1$). Note that this is a restriction inherent to Young's equation, which strictly is not valid when $\Delta\gamma/\gamma > 1$. However, there are no physical reasons for why this cannot be the case. It simply means that Young's equation is not applicable in the complete wetting regime.

21967350, 0, Downloaded from https://advanced.onlinelibrary.wiley.com/doi/10.1002/admi.70698 by CochraneItalia, Wiley Online Library on [07/10/2026]. See the Terms and Conditions (https://onlinelibrary.wiley.com/terms-and-conditions) on Wiley Online Library for rules of use; OA articles are governed by the applicable Creative Commons License

TABLE 1 | Comparison of simulation results using two independent methods for investigating wetting.

	Droplet simulations		Potential of mean force simulations			
Surface	θ (degrees)	cos θ	W_A (mJ m^{-2})	$\Delta\gamma/\gamma$	S (mJ m^{-2})	θ (degrees)
Native hydrophilic (110)	0°	1	136	1.32	19	0°
Native hydrophobic (200)	20°	0.94	115	0.96	−2	18°
Acetylated	30°	0.87	123	1.09	6	0°
TEMPO oxidized	0°	1	378	5.44	261	0°

There are several interesting observations with respect to effects from surface chemistry. The work of adhesion follows the order TEMPO > Native hydrophilic > Acetylated > Native hydrophobic, which aligns with going from charged to polar to less polar. Native cellulose has both hydrophilic and hydrophobic characteristics, depending on which crystallographic plane is considered. Water wets the (110) plane completely and forms a static contact angle on the (200) plane, yet below 90°. For a cellulose fibril, the ratio of hydrophobic surface to hydrophilic depends on which cross section is assumed, but it is in every case likely to be below 1. For the hexagonal 18 chain model commonly assumed for wood cellulose [48], it is approximately 0.5. It means there are more hydrophilic than hydrophobic surfaces. In addition, if there are residual cell wall polymers present (e.g., hemicellulose) the hydrophobic surfaces are the most likely adsorption sites [49], effectively reducing the available hydrophobic surface area.

In technical applications, cellulose is often functionalized. Our simulations show that TEMPO oxidation leads to increased hydrophilicity, with a considerably larger spreading coefficient than for the Native hydrophilic surface, 261 mJ m^{-2} compared to 19 mJ m^{-2}. This correlates with the higher moisture sorption of nanocellulose films from TEMPO-oxidized fibrils compared with native cellulose films [50]. Our simulations also show hydrophobization effects from acetylation: the Acetylated surface shows the largest wetting angle (30°) calculated by droplet method, and $\Delta\gamma/\gamma$ falls below the value for Native hydrophilic, but above the value for Native hydrophobic. Experimentally, acetylation leads to significantly reduced moisture sorption in acetylated cellulose nanopapers compared to unmodified ones [14], and to reduced hygroscopicity in bacterial cellulose nanocomposites [51].

Overall, contact angles for the native hydrophobic substrate agree reasonably well between the droplet simulations and the PMF approach, but it is *smaller* in the latter case. The same is true for the acetylated surface, where the droplet simulation gives a static contact angle while the PMF predicts complete wetting. Either the droplet simulations overestimate the contact angle or the PMF is underestimating it. We will return to this issue.

As was mentioned in the introduction, there are several published studies on the topic of cellulose wetting, both experimental and computational. Static contact angles determined from MD vary greatly due to different simulation protocols. Even relative comparisons need attention to detail, large systems, and sufficient simulation time to reach equilibrium. The choice of water model, particularly its liquid surface tension, influences the results. Karna et al. [25] used the same combination of carbohydrate force field and water model as in the present study and simulated a contact angle of 42° on the hydrophilic face of cellulose. However, their reported value for the SPC/E liquid surface tension was 67.5 mJ m^{-2}, which is significantly higher than the value obtained here. The surface tension of common water models vary between around 50 mJ m^{-2} to close to the experimental value of 72 mJ m^{-2}, but they also depend strongly on simulation protocol [47]. For the SPC/E model at 300 K, we have previously [28] reported a value of 58.6 mJ m^{-2}, and Chen and Smith [47] obtained 56.7 mJ m^{-2}. With $\cos\theta = \Delta\gamma/\gamma$, the θ angle becomes sensitive to the exact value of the surface tension, and we note that the predicted contact angles would be larger with a more realistic value for γ. However, switching the water model from the three-site SPC/E to two slightly more expensive but also more accurate four-site models, TIP4P/2005 [52] and OPC [53], which have surface tensions 61.8 and 67.1 mJ m^{-2} using the present simulation conditions, still leads to complete wetting of the Native hydrophilic surface in less than 100 ns (Figure S2).

3.3 | The Dynamics of Cellulose Wetting

Non-equilibrium wetting is in practice important for cellulose materials. For instance, the kinetics of wetting is important during many industrial processes, e.g. involving hydrocolloids or water solutions. The dynamics of wetting, e.g., the velocity by which the liquid spreads on the substrate, will depend strongly on liquid-substrate interactions and is of particular interest here. For hydrogen bonding systems, such as water spreading on a polar surface, the strong (compared to thermal energy) and directional nature of the bonds between the liquid and the substrate inhibit liquid slip. On a fundamental level, this makes general hydrodynamic theory incompatible with an advancing contact line [54]. This can be resolved by introducing an energy dissipating mechanism at the contact line itself, termed the contact line friction, μ_f, which has the dimension of viscosity. The contact line friction gives rise to a friction term in its normal mechanical sense, which appears in the equation of motion for the contact line. It depends on both liquid-substrate interactions and viscous interactions between liquid molecules close to the contact line [55]. It has been shown that by accounting for contact line friction, the dynamics of droplet spreading could be rationalized for a large number of liquid-substrate combinations, varying in both viscosity and surface chemistry (e.g. hydrogen bonding) [56]. For this reason, analyzing contact line friction is relevant for cellulose-water investigations.

Figure 4 shows interesting time evolution of the wetting radii of water droplets from our simulations. We consider two regions, $1 < t < 10$ ns and $10 < t < 100$ ns. The first region corresponds

21967350, 0, Downloaded from https://advanced.onlinelibrary.wiley.com/doi/10.1002/admi.70698 by CochraneItalia, Wiley Online Library on [07/10/2026]. See the Terms and Conditions (https://onlinelibrary.wiley.com/terms-and-conditions) on Wiley Online Library for rules of use; OA articles are governed by the applicable Creative Commons License

to the early stages of spreading and the development of a spherical cap (see Figure 2). Here the system has passed the initial (very rapid) spreading but is still far from equilibrium. The evolution of the wetting radii on all substrates is close to a $t^{1/2}$ dependence (dashed lines in Figure 4). In the later stage ($t > 10$ ns), the time evolution changes and the spreading on the hydrophobic substrates slows down significantly as the droplets approach their equilibrium shapes. Here the scaling with time is approximately $t^{1/7}$ as predicted in the hydrodynamic regime for a cylindrical geometry [57] (the 2D version of Tanner's law). For the completely wetting substrates, however, the spreading does not stop until the contact line meets the boundary of the periodic box. This behavior is consistent with the contact-line-friction-dominated regime proposed by Carlson, Bellani and Amberg [56], with the subsequent exponents, 0.17 and 0.13, suggesting a crossover from localized contact-line dissipation to predominantly hydrodynamic dissipation. Following Carlson et al., [56] an estimate for the transition time can be obtained by equating the friction-dominated time scale with the hydrodynamic spreading, $(\gamma t/R\mu_f)^{1/2} = (\gamma t/R\mu)^{1/7}$, leading to

$$t_t = \frac{R\mu_f}{\gamma}\left(\frac{\mu_f}{\mu}\right)^{\frac{2}{5}} \tag{4}$$

differing only in the exponent compared to the result for axisymmetric droplets. To test this prediction, a value for the contact line friction is needed.

The liquid spreading is the fastest on the charged TEMPO-oxidized surface, followed by the native hydrophilic one. This suggests that charge and polar interactions provide a strong driving force for water spreading, which aligns with the simplified notion of hydrophilicity. The spreading velocities on the two hydrophobic surfaces (Acetylated and Native hydrophobic) are notably smaller, since interactions are less favorable. Interestingly, spreading velocity is the smallest on the Acetylated surface, despite the native hydrophobic having a lower W_A (Table 1). Thus, the thermodynamics alone, or the continuum models derived from fluid dynamics are not enough to describe motion at small scale.

Molecular kinetic (MK) theory [58] describes the molecular origin behind the contact line motion as thermally activated molecular "jumps" where liquid molecules move from one potential well to another. In our case, this broadly corresponds to water molecules shifting hydrogen-bonding partners (polar groups on the substrate or other liquid molecules). Within this framework, the contact line velocity, $v(t)$, can be related to the forces acting on the contact line, $F(t)$, and the friction [59],

$$v\ (t) = \frac{F\,(t)}{\mu_f} = \frac{\gamma}{\mu_f}\ (\cos\theta_0 - \cos\theta\,(t)) = \frac{\gamma}{\mu_f}\ \left(\frac{\Delta\gamma}{\gamma} - \cos\theta\,(t)\right) \tag{5}$$

Since $v(t)$ and $\cos\theta(t)$ can be measured in MD simulations, and $\cos\theta_0$ refers to the equilibrium wetting angle, which for the case of complete wetting is replaced by $\Delta\gamma/\gamma \geq 1$, the friction μ_f can be calculated from the simulation trajectories.

It was previously assumed that μ_f is a material constant of the specific liquid-substrate interface, but MD simulations have shown that it depends on $v(t)$, and specifically that it increases with decreasing velocity [32, 54]. However, the size of the droplets used in this study were relatively small, which severely limits the precision compared to the previous studies. Thus, μ_f calculated from our trajectories using Equation 5 at different stages of spreading show large variation (Figure S3), and we instead compute the average friction coefficients over the first 10 ns (Table 2). Their magnitudes, here normalized to the viscosity of the water model [60] (0.73 mPa s), agree well with both MD simulations [32] and experimental/modelling results [56] for water on hydrophilic silica.

The friction coefficient is largest on the charged surface, followed by the polar one. This is consistent with the notion of strong intermolecular forces at the liquid-solid interface. As the average surface forces become smaller by having lower density of polar groups (as in the native hydrophobic surface) or by reducing the polarity of the surface groups (by acetylation) the friction coefficient becomes smaller (although the observed difference between Native hydrophilic and Acetylated is not statistically significant). Importantly, the friction coefficients are in all cases at least one order of magnitude larger than the viscosity of liquid water. The calculated friction coefficients inserted in Equation 4 give the estimated transition time between friction dominated spreading and the hydrodynamic regime. It becomes 7 ns for the native hydrophobic surface, and 15 ns for the acetylated one. These values agree well with the behavior shown in Figure 5, indicating good internal consistency of our analysis. Thus, effects from contact line friction must be accounted for as an energy dissipation mechanism in these systems, which we will attempt to quantify in the following.

The energy dissipation due to friction at the contact line can be written as [56, 61]

$$\dot{E}_\mu = 2w\mu_f v^2 \tag{6}$$

where w is the width of the substrate (i.e., the length of the contact line). Following Johansson and Hess [32], the rate of total energy change in the system is

$$\dot{E}_\gamma = w\left(2v\Delta\gamma - \gamma\,\dot{s}\right) \tag{7}$$

Here $\dot{s}$ is the rate of change for the length of the liquid-vapor interface, which is calculated from the time dependence of $s = 2\theta r/\sin\theta$. Combining Equations 6 and 7, we calculate the contribution from friction to the total energy dissipation as the ratio $\dot{E}_\mu\dot{E}_\gamma$, averaged over the first 10 ns (Table 2). This contribution is substantial, averaging to between 65% and 88% for the different substrates, demonstrating that contact line friction is indeed the dominating contribution to energy dissipation in water/cellulose wetting at this scale.

As was noted above, the most significant discrepancy between contact angles computed by either the droplet simulations or by PMF was for the acetylated surface, for which the first method gave an equilibrium contact angle of 30°, and the second method predicted complete wetting. This may be rationalized by considering the microscopic details of the interface. As θ becomes smaller, the spreading velocity decreases (Figure 5) until the

21967350, 0, Downloaded from https://advanced.onlinelibrary.wiley.com/doi/10.1002/admi.70698 by CochraneItalia, Wiley Online Library on [07/10/2026]. See the Terms and Conditions (https://onlinelibrary.wiley.com/terms-and-conditions) on Wiley Online Library for rules of use; OA articles are governed by the applicable Creative Commons License

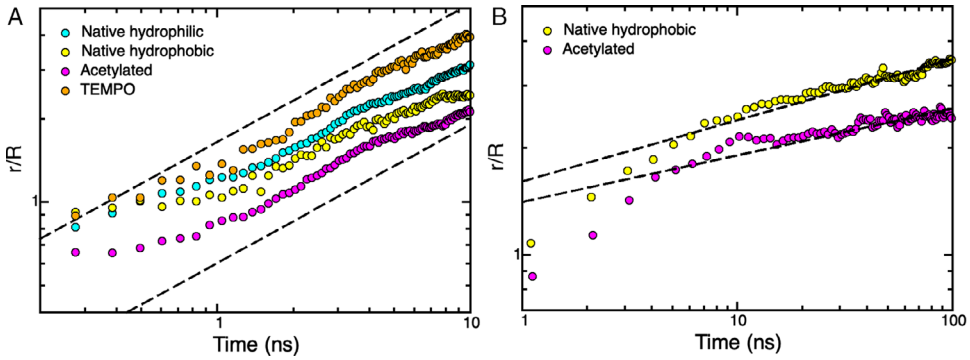

FIGURE 5 | (A) Time evolution of the wetting radius for the early stage of spreading of a water droplet on different cellulose substrates. Importantly, the dashed lines indicates a $t^{1/2}$ time dependence. (B) Time evolution at a later stage for spreading on the more hydrophobic substrates. The dashed lines are fits to the data and has the slopes of 0.17 and 0.13 for the native and acetylated substrates, respectively, which is close to 1/7 as predicted for the hydrodynamic regime.

TABLE 2 | Average friction coefficients (in units of water viscosity) over the first 10 ns with standard errors; Ratio of contact line energy dissipation to total.

	μ_f/μ_w	$\dot{E}_\mu\dot{E}_\gamma$
Native hydrophilic	55.7 ± 5.2	0.88
Native hydrophobic	30.5 ± 6.2	0.82
Acetylated	52.4 ± 8.7	0.65
TEMPO oxidized	216.5 ± 27.7	0.77

motion of the contact line, for the case of hydrophobic substrates, eventually stops. Mechanistically, this is a consequence of a vanishing driving force, $F(t)$, as theta approaches θ_0 (Equation 5). However, in a picture where the contact line advances by "jumps" between adsorption sites, as in the MK theory, the velocity can become zero before the equilibrium is attained. This may occur when the activation energy for moving between adsorption sites is large compared to thermal energy, as could be the case for chemically heterogeneous surfaces and/or interfaces with high surface roughness. The consequence is that the static contact angle is different from the equilibrium contact angle. This phenomenon is termed contact line pinning and has been observed at the nanoscale both in experiments [62, 63] and MD simulations [64], although not yet for cellulosic substrates.

Cellulose is inherently patchy, with alternating hydrophobic and hydrophilic moieties [65]. The patchiness is further enhanced by hydrophobic substitutions, such as acetylation, which, being comparably bulky, also contributes to the (molecular) surface roughness. The activation energy needed to move past such hydrophobic substitution could, potentially, be relatively large. Thus, we speculate that this leads to pinning of the contact line in the simulations of acetylated surfaces, which can explain why the final θ measured from the droplet simulations are larger than θ derived from the PMF simulations. However, it would be of interest to investigate this phenomenon using larger droplets to spot a possible size dependence, and perhaps in a full 3D geometry instead of the cylindrical droplets used here, to find out if this would be of any real concern for liquid spreading in cellulose nanofibril networks. However, since many liquid transport processes of concern for cellulose materials, such as moisture transport in wood or monomer infiltration of fibril networks, take place far from equilibrium, the analysis of wetting dynamics in the early stages of droplet spreading is useful. Our simulations show large differences between substrates of different chemistry where introduction of charge leads to enhanced wetting by water. This is quantitatively shown by the larger $\Delta\gamma/\gamma$, which is recognized as the (substrate specific) driving force for advancing the contact line. This parameter can thus be directly linked to the transport of water in nanopores and ultimately swelling of cellulose nanomaterials. However, the spreading is slowed down by the contact line friction, and this effect is probably much larger in real material systems which do not consist of the large, molecularly smooth, surfaces used in the simulations.

As was mentioned in the introduction, a direct comparison between simulated wetting and experiments is not straightforward. Experimentally determined contact angles on cellulose are heavily influenced by macroscopic effects (surface roughness and heterogeneity, and absorption) while MD simulations operate on the nanoscale, which indeed introduces artifacts due to the small size and short time scales. By using larger systems and extending our simulations to longer times than previously, simulated contact angles were notably smaller than most reported literature values, which illustrates this point. One possible path forward to make simulations and experiments meet is to use meso-scale models which can be simulated by, e.g., computational fluid dynamics methods, as was demonstrated for the case of glass substrates [55] and silica [56]. While such models can be made to take macroscopic features into account, they do not incorporate the atomistic details of the liquid-substrate interactions. Thus, atomistic MD simulations could be useful for providing realistic

21967350, 0, Downloaded from https://advanced.onlinelibrary.wiley.com/doi/10.1002/admi.70698 by Cochraneltalia, Wiley Online Library on [07/10/2026]. See the Terms and Conditions (https://onlinelibrary.wiley.com/terms-and-conditions) on Wiley Online Library for rules of use; OA articles are governed by the applicable Creative Commons License

input (such as microscopic surface energies or contact line friction coefficients) for simulations on larger scales. While the results presented herein shows that the wetting behavior is consistent between several water models, one important caveat is that the choice of force field parameters for the cellulose substrate may affect simulated contact angles. It is known for instance that the carbohydrate force field employed here consistently gives stronger adsorption in single molecule adsorption simulations than other force fields. As one example, MD simulations of xylo-oligomers on cellulose surfaces in water show stable adsorption with GLYCAM06 [66], while simulations with CHARMM under similar conditions may even give spontaneous desorption [67]. This imbalance could possibly apply to cellulose-water interactions as well and should be systematically investigated in the future.

4 | Conclusions

Our simulations of water droplets spreading on cellulose substrates show that wetting of cellulose depends on surface chemistry. Native cellulose is hygroscopic, and water wets the "hydrophilic" surfaces completely, and even the "hydrophobic" surfaces are partially wetted with an equilibrium contact angle of ∼20°. TEMPO oxidation leads to even more efficient wetting due to the presence of surface charge, whereas acetylation is effectively a hydrophobization, reducing the wetting efficiency.

Contact angles of water on cellulose substrates computed from molecular dynamics simulations are sensitive to details. Previously the choice of force field parameters, in particular the water model, and system size was shown to affect the result. In the present study we have shown that also the total simulation time is an important factor to consider. In simulations of explicit nano droplets, spreading slows down significantly as the equilibrium contact angle is approached, and simulations longer than 100 ns was needed here to determine whether it had come to a halt or not. As an alternative, contact angles were calculated from the work of adhesion, simulated using umbrella sampling. Convergence was assessed by systematically increase the simulation time in each umbrella window, showing that simulations of, at least, tens of nanoseconds are needed. The fact that much smaller systems can be used in this approach makes it more computationally efficient than simulating explicit droplets. In addition, this method has the additional advantages that it (i) removes possible dependencies on droplet size, (ii) discriminates between the wetting efficiency even in the completely wetting regime since it is not limited by having $\cos\theta \leq 1$, and (iii) gives the "true" equilibrium static contact angle without hysteresis effects, such as contact line pinning, which we demonstrate can originate from molecular-scale surface heterogeneity.

To study the dynamics of wetting, the method with explicit droplets is, however, the only alternative. The spreading velocity depends strongly on liquid-substrate interactions, and it was found to be faster on more hydrophilic substrates. It was, however, slower on the acetylated surface than the native hydrophobic one, despite it being more hydrophilic as judged from the contact angle. This shows that equilibrium properties are not sufficient to describe this non-equilibrium process. In all cases, the spreading radius was found to scale with $t^{1/2}$, which is indicative of a process where friction at the contact line is an important energy dissipation mechanism. By analyzing the contact line motion within the framework of molecular kinetic theory, it was found that contact line friction contributed 70%–90% of the total energy dissipation.

Given the challenges of performing cellulose wetting experiments systematically, for instance due to the difficulty of producing well-characterized model substrates, computer simulation is an attractive option to study wettability, especially on the nano scale. We have shown that if convergence is carefully assessed, molecular dynamics provide quantitative predictions of key parameters that, for example, can be useful for modeling on larger scales. The results will also increase our general understanding of liquid imbibition of cellulose networks, which is important for many material processing methods.

Author Contributions

Jakob Wohlert: conceptualization, investigation, Writing – original draft, formal analysis. **Lars Berglund**: conceptualization, writing – review and editing.

Acknowledgements

The AI-TranspWood project, HORIZON-CL4–2023-RESILIENCE-01–23 (Grant Agreement 101138191), is gratefully acknowledged. This project is co-funded by the European Union. Views and opinions expressed are however those of the author(s) only and do not necessarily reflect those of the European Union or HaDEA. Neither the European Union nor the granting authority can be held responsible for them. The computations were enabled by resources provided by the National Academic Infrastructure for Supercomputing in Sweden (NAISS), partially funded by the Swedish Research Council through grant agreement no. 2022–06725.

Conflicts of Interest

The authors declare no conflicts of interest.

Data Availability Statement

The data that support the findings of this study are available from the corresponding author upon reasonable request.

References

1. M. M. Hamedi, M. Sandberg, R. T. Olsson, J. Pedersen, T. Benselfelt, and J. Wohlert, "Wood and Cellulose: The Most Sustainable Advanced Materials for Past, Present, and Future Civilizations," *Advanced Materials* 37 (2025): 2415787.

2. C. Chen, L. Berglund, I. Burgert, and L. Hu, "Wood Nanomaterials and Nanotechnologies," *Advanced Materials* 33, no. 28 (2021): 2006207.

3. L. Solhi, V. Guccini, K. Heise, et al., "Understanding Nanocellulose–Water Interactions: Turning a Detriment Into an Asset," *Chemical Reviews* 123, no. 5 (2023): 1925–2015.

4. A. Etale, A. J. Onyianta, S. R. Turner, and S. J. Eichhorn, "Cellulose: A Review of Water Interactions, Applications in Composites, and Water Treatment," *Chemical Reviews* 123, no. 5 (2023): 2016–2048.

5. D. J. Cosgrove, "Structure and Growth of Plant Cell Walls," *Nature Reviews Molecular Cell Biology* 25, no. 5 (2024): 340–358.

6. M. Henriksson, L. A. Berglund, P. Isaksson, T. Lindström, and T. Nishino, "Cellulose Nanopaper Structures of High Toughness," *Biomacromolecules* 9, no. 6 (2008): 1579–1585.

21967350, 0, Downloaded from https://advanced.onlinelibrary.wiley.com/doi/10.1002/admi.70698 by CochraneItalia, Wiley Online Library on [07/10/2026]. See the Terms and Conditions (https://onlinelibrary.wiley.com/terms-and-conditions) on Wiley Online Library for rules of use; OA articles are governed by the applicable Creative Commons License

7. M. Wohlert, T. Benselfelt, L. Wågberg, I. Furó, L. A. Berglund, and J. Wohlert, "Cellulose and the Role of Hydrogen Bonds: Not in Charge of Everything," *Cellulose* 29 (2022): 1–23.

8. E. L. Lindh, C. Terenzi, L. Salmén, and I. Furó, "Water in Cellulose: Evidence and Identification of Immobile and Mobile Adsorbed Phases by 2H MAS NMR," *Physical Chemistry Chemical Physics* 19 (2017): 4360–4369.

9. M. N. Belgacem and A. Gandini, "The Surface Modification of Cellulose Fibres for Use as Reinforcing Elements in Composite Materials," *Composite Interfaces* 12 (2005): 41–75.

10. S. Eyley and W. Thielemans, "Surface Modification of Cellulose Nanocrystals," *Nanoscale* 6 (2014): 7764–7779.

11. S. Ifuku, M. Nogi, K. Abe, K. Handa, F. Nakatsubo, and H. Yano, "Surface Modification of Bacterial Cellulose Nanofibers for Property Enhancement of Optically Transparent Composites: Dependence on Acetyl-Group DS," *Biomacromolecules* 8 (2007): 1973–1978.

12. A. Isogai, T. Saito, and H. Fukuzumi, "TEMPO-Oxidized Cellulose Nanofibers," *Nanoscale* 3 (2011): 71–85.

13. S. Spinella, G. Lo Re, B. Liu, et al., "Polylactide/Cellulose Nanocrystal Nanocomposites: Efficient Routes for Nanofiber Modification and Effects of Nanofiber Chemistry on PLA Reinforcement," *Polymer* 65 (2015): 9–17.

14. A. G. Cunha, Q. Zhou, P. T. Larsson, and L. A. Berglund, "Topochemical Acetylation of Cellulose Nanopaper Structures for Biocomposites: Mechanisms for Reduced Water Vapour Sorption," *Cellulose* 21 (2014): 2773–2787.

15. P. Chen, J. Wohlert, L. Berglund, and I. Furó, "Water as an Intrinsic Structural Element in Cellulose Fibril Aggregates," *The Journal of Physical Chemistry Letters* 13 (2022): 5424–5430.

16. A. Y. Mehandzhiyski, M.-X. Ruiz-Caldas, P. Heasman, V. Apostolopoulou-Kalkavoura, L. Bergström, and I. Zozoulenko, "Is it Possible to Completely Dry Cellulose?," *Carbohydrate Polymers* 365 (2025): 123803.

17. P. G. de Gennes, "Wetting: Statics and Dynamics," *Reviews of Modern Physics* 57, no. 3 (1985): 827–863.

18. J. Lu, P. Askeland, and L. T. Drzal, "Surface Modification of Microfibrillated Cellulose for Epoxy Composite Applications," *Polymer* 49, no. 5 (2008): 1285–1296.

19. M. Mashkour, E. Afra, H. Resalati, and M. Mashkour, "Moderate Surface Acetylation of Nanofibrillated Cellulose for the Improvement of Paper Strength and Barrier Properties," *RSC Advances* 5, no. 74 (2015): 60179–60187.

20. K. Xhanari, K. Syverud, G. Chinga-Carrasco, K. Paso, and P. Stenius, "Reduction of Water Wettability of Nanofibrillated Cellulose by Adsorption of Cationic Surfactants," *Cellulose* 18, no. 2 (2011): 257–270.

21. A. Lozhechnikova, D. Dax, J. Vartiainen, S. Willför, C. Xu, and M. Österberg, "Modification of Nanofibrillated Cellulose Using Amphiphilic Block-Structured Galactoglucomannans," *Carbohydrate Polymers* 110 (2014): 163–172.

22. M. S. Peresin, K. Kammiovirta, H. Heikkinen, et al., "Understanding the Mechanisms of Oxygen Diffusion Through Surface Functionalized Nanocellulose Films," *Carbohydrate Polymers* 174 (2017): 309–317.

23. E. Kontturi, M. Suchy, P. Penttilä, et al., "Amorphous Characteristics of an Ultrathin Cellulose Film," *Biomacromolecules* 12, no. 3 (2011): 770–777.

24. K. Mazeau and A. Rivet, "Wetting the (110) and (100) Surfaces of Iβ Cellulose Studied by Molecular Dynamics," *Biomacromolecules* 9, no. 4 (2008): 1352–1354.

25. N. K. Karna, J. Wohlert, A. Lidén, T. Mattsson, and H. Theliander, "Wettability of Cellulose Surfaces Under the Influence of an External Electric Field," *Journal of Colloid and Interface Science* 589 (2021): 347–355.

26. L. N. Trentin, C. S. Pereira, R. L. Silveira, S. Hill, M. Sorieul, and M. S. Skaf, "Nanoscale Wetting of Crystalline Cellulose," *Biomacromolecules* 22, no. 10 (2021): 4251–4261.

27. Y. Wang, A. Kiziltas, P. Blanchard, and T. R. Walsh, "ContactAngleCalculator: An Automated, Parametrized, and Flexible Code for Contact Angle Estimation in Visual Molecular Dynamics," *Journal of Chemical Information and Modeling* 62, no. 24 (2022): 6302–6308.

28. A. S. Sridhar, L. A. Berglund, and J. Wohlert, "Wetting of Native and Acetylated Cellulose by Water and Organic Liquids From Atomistic Simulations," *Cellulose* 30, no. 13 (2023): 8089–8106.

29. D. C. Malaspina and J. Faraudo, "Molecular Insight Into the Wetting Behavior and Amphiphilic Character of Cellulose Nanocrystals," *Advances in Colloid and Interface Science* 267 (2019): 15–25.

30. R. C. Tolman, "The Effect of Droplet Size on Surface Tension," *The Journal of Chemical Physics* 17, no. 3 (1949): 333–337.

31. M. Kanduč, L. Eixeres, S. Liese, and R. R. Netz, "Generalized line Tension of Water Nanodroplets," *Physical Review E* 98, no. 3 (2018): 032804.

32. P. Johansson and B. Hess, "Molecular origin of contact line Friction in Dynamic Wetting," *Physical Review Fluids* 3 (2018): 074201.

33. N. Di Pasquale, J. Algaba, P. M. D. Hijes, et al., "Solid–Liquid Interfacial Free Energy From Computer Simulations: Challenges and Recent Advances," *Chemical Reviews* 125, no. 10 (2025): 5003–5053.

34. J. G. Kirkwood and F. P. Buff, "The Statistical Mechanical Theory of Surface Tension," *The Journal of Chemical Physics* 17, no. 3 (1949): 338–343.

35. J. J. Hoyt, M. Asta, and A. Karma, "Method for Computing the Anisotropy of the Solid-Liquid Interfacial Free Energy," *Physical Review Letters* 86, no. 24 (2001): 5530–5533.

36. Y. Okita, T. Saito, and A. Isogai, "Entire Surface Oxidation of Various Cellulose Microfibrils by TEMPO-Mediated Oxidation," *Biomacromolecules* 11 (2010): 1696–1700.

37. K. N. Kirschner, A. B. Yongye, S. M. Tschampel, et al., "GLYCAM06: A Generalizable Biomolecular Force Field. Carbohydrates," *Journal of Computational Chemistry* 29 (2008): 622–655.

38. H. J. C. Berendsen, J. R. Grigera, and T. P. Straatsma, "The Missing Term in Effective Pair Potentials," *The Journal of Physical Chemistry* 91 (1987): 6269–6271.

39. T. Saito, Y. Nishiyama, J.-L. Putaux, M. Vignon, and A. Isogai, "Homogeneous Suspensions of Individualized Microfibrils From TEMPO-Catalyzed Oxidation of Native Cellulose," *Biomacromolecules* 7 (2006): 1687–1691.

40. I. S. Joung and T. E. Cheatham III, "Determination of Alkali and Halide Monovalent Ion Parameters for Use in Explicitly Solvated Biomolecular Simulations," *The Journal of Physical Chemistry B* 112, no. 30 (2008): 9020–9041.

41. S. Páll, A. Zhmurov, P. Bauer, et al., "Heterogeneous Parallelization and Acceleration of Molecular Dynamics Simulations in GROMACS," *The Journal of Chemical Physics* 153, no. 13 (2020): 134110.

42. B. Hess, "P-LINCS: A Parallel Linear Constraint Solver for Molecular Simulation," *Journal of Chemical Theory and Computation* 4 (2008): 116–122.

43. T. Darden, D. York, and L. P. M. E. Pedersen, "Particle Mesh Ewald: An N·log(N) Method for Ewald Sums in Large Systems," *The Journal of Chemical Physics* 98 (1993): 10089–10092.

44. U. Essmann, L. Perera, M. L. Berkowitz, T. Darden, H. Lee, and L. G. Pedersen, "A Smooth Particle Mesh Ewald Method," *The Journal of Chemical Physics* 103 (1995): 8577–8593.

45. G. Bussi, D. Donadio, and M. Parrinello, "Canonical Sampling Through Velocity Rescaling," *The Journal of Chemical Physics* 126 (2007): 014101.

46. J. S. Hub, B. L. De Groot, and D. Van Der Spoel, "g_wham—A Free Weighted Histogram Analysis Implementation Including Robust Error and Autocorrelation Estimates," *Journal of Chemical Theory and Computation* 6, no. 12 (2010): 3713–3720.

21967350, 0, Downloaded from https://advanced.onlinelibrary.wiley.com/doi/10.1002/admi.70698 by Cochraneltalia, Wiley Online Library on [07/10/2026]. See the Terms and Conditions (https://onlinelibrary.wiley.com/terms-and-conditions) on Wiley Online Library for rules of use; OA articles are governed by the applicable Creative Commons License

47. F. Chen and P. E. Smith, "Simulated Surface Tensions of Common Water Models," *The Journal of Chemical Physics* 126, no. 22 (2007): 221101.

48. K. Daicho, T. Saito, S. Fujisawa, and A. Isogai, "The Crystallinity of Nanocellulose: Dispersion-Induced Disordering of the Grain Boundary in Biologically Structured Cellulose," *ACS Applied Nano Materials* 1 (2018): 5774–5785.

49. E. Heinonen, G. Henriksson, M. E. Lindström, F. Vilaplana, and J. Wohlert, "Structure of Plant Cell Wall Oligosaccharides Defines Their Interaction With Cellulose Microfibrils," *Cellulose* 33, no. 4 (2026): 1905–1925.

50. X. Yang, E. Jungstedt, M. S. Reid, and L. A. Berglund, "Polymer Films From Cellulose Nanofibrils—Effects From Interfibrillar Interphase on Mechanical Behavior," *Macromolecules* 54, no. 9 (2021): 4443–4452.

51. M. Nogi, K. Abe, K. Handa, F. Nakatsubo, S. Ifuku, and H. Yano, "Property Enhancement of Optically Transparent Bionanofiber Composites by Acetylation," *Applied Physics Letters* 89 (2006): 233123.

52. J. L. F. Abascal and C. Vega, "A General Purpose Model for the Condensed Phases of Water: TIP4P/2005," *The Journal of Chemical Physics* 123, no. 23 (2005): 234505.

53. S. Izadi, R. Anandakrishnan, and A. V. Onufriev, "Building Water Models: A Different Approach," *The Journal of Physical Chemistry Letters* 5, no. 21 (2014): 3863–3871.

54. M. Pellegrino and B. Hess, "Asymmetry of Wetting and De-Wetting on High-Friction Surfaces Originates From the Same Molecular Physics," *Physics of Fluids* 34, no. 10 (2022): 102010.

55. D. Duvivier, D. Seveno, R. Rioboo, T. D. Blake, and J. De Coninck, "Experimental Evidence of the Role of Viscosity in the Molecular Kinetic Theory of Dynamic Wetting," *Langmuir* 27, no. 21 (2011): 13015–13021.

56. A. Carlson, G. Bellani, and G. Amberg, "Universality in Dynamic Wetting Dominated by Contact-Line Friction," *Physical Review E* 85, no. 4 (2012): 045302.

57. D. R. Heine, G. S. Grest, and E. B. Webb, "Spreading Dynamics of Polymer Nanodroplets in cylindrical geometries," *Physical Review E* 70, no. 1 (2004): 011606.

58. T. D. Blake and J. M. Haynes, "Kinetics of Displacement," *Journal of Colloid and Interface Science* 30, no. 3 (1969): 421–423.

59. G. Amberg, "Detailed Modelling of Contact Line Motion in Oscillatory Wetting," *npj Microgravity* 8, no. 1 (2022): 1.

60. M. A. González and J. L. Abascal, "The Shear Viscosity of Rigid Water Models," *The Journal of Chemical Physics* 132, no. 9 (2010): 096101.

61. M. J. De Ruijter, J. De Coninck, and G. Oshanin, "Droplet Spreading: Partial Wetting Regime Revisited," *Langmuir* 15, no. 6 (1999): 2209–2216.

62. L. Du, H. Bodiguel, and A. Colin, "Thermally Activated Depinning Motion of Contact Lines in Pseudopartial Wetting," *Physical Review E* 90, no. 1 (2014): 012402.

63. M. Ramiasa, J. Ralston, R. Fetzer, et al., "Contact Line Motion on Nanorough Surfaces: A Thermally Activated Process," *Journal of the American Chemical Society* 135, no. 19 (2013): 7159–7171.

64. F.-C. Wang and H.-A. Wu, "Pinning and depinning Mechanism of the Contact Line During Evaporation of Nano-Droplets Sessile on Textured Surfaces," *Soft Matter* 9, no. 24 (2013): 5703–5709.

65. O. Biermann, E. Hädicke, S. Koltzenburg, and F. Müller-Plathe, "Hydrophilicity and Lipophilicity of Cellulose Crystal Surfaces," *Angewandte Chemie International Edition* 40, no. 20 (2001): 3822–3825.

66. E. Heinonen, G. Henriksson, M. E. Lindström, F. Vilaplana, and J. Wohlert, "Xylan Adsorption on Cellulose: Preferred Alignment and Local Surface Immobilizing Effect," *Carbohydrate Polymers* 285 (2022): 119221.

67. M. Gupta, T. B. Rawal, P. Dupree, J. C. Smith, and L. Petridis, "Spontaneous Rearrangement of Acetylated Xylan on Hydrophilic Cellulose Surfaces," *Cellulose* 28, no. 6 (2021): 3327–3345.

Supporting Information

Additional supporting information can be found online in the Supporting Information section.

Supporting File: admi70698-sup-0001-SuppMat.docx.

21967350, 0, Downloaded from https://advanced.onlinelibrary.wiley.com/doi/10.1002/admi.70698 by CochraneItalia, Wiley Online Library on [07/10/2026]. See the Terms and Conditions (https://onlinelibrary.wiley.com/terms-and-conditions) on Wiley Online Library for rules of use; OA articles are governed by the applicable Creative Commons License